공학석사학위논문

Two Novel Cholesteric Liquid Crystal Systems: Microfluidics-Produced Droplets and Self-Assembled Cellulose Nanocrystal Films

새로운 콜레스테릭 액정 시스템의 제시: 미세 유체 시스템을 이용한 액정 방울과 자가 조립으로 형성된 나노셀룰로오스 필름에 관한 연구

2014 년 2 월

서울대학교 대학원

융합과학부 나노융합전공

노 정 현

Two Novel Cholesteric Liquid Crystal Systems: Microfluidics-Produced Droplets and Self-Assembled Cellulose Nanocrystal Films

새로운 콜레스테릭 액정 시스템의 제시:
미세 유체 시스템을 이용한 액정 방울과
자가 조립으로 형성된 나노셀룰로오스 필름에 관한 연구

지도교수 Jan Lagerwall
이 논문을 공학석사학위논문으로 제출함

2014년 2월

서울대학교 대학원
융합과학부 나노융합전공
노 정 현

노정현의 석사학위논문을 인준함
2014년 2월

위 원 장 김 연 상 (인)
부 위 원 장 Jan Lagerwall (인)
위 원 송 윤 규 (인)

Abstract

Two Novel Cholesteric Liquid Crystal Systems: Microfluidics-Produced Droplets and Self-Assembled Cellulose Nanocrystal Films

JungHyun Noh
Department of Transdisciplinary Studies
(Program in Nano Science & Technology)
The Graduate School
Seoul National University

Cholesteric (N*) liquid crystals have attracted much attention over a broad research field thanks to their peculiar optical properties, rendering them exquisite soft photonic materials. The period of their self-assembled helical structure can be tuned to reflect light in any part of the visible spectrum by adjusting chemical composition or temperature. The helical arrangement of the building blocks of the phase also gives the reflected light circular polarization with same handedness as the helix. Here we focus on two modern cholesteric systems and the unique optical properties that they develop: monodisperse cholesteric liquid crystal droplets and dried films of cellulose nanocrystals with a vitrified internal cholesteric structure.

With a coaxial microfluidic set-up we produce monodisperse droplets of suitable cholesteric mixtures, dispersed in a dilute aqueous polyvinylalcohol (PVA) and glycerol solution as continuous phase. The droplets are collected at such high

volume fraction that they spontaneously organize into a 2D colloidal crystal arrangement. The continuous phase composition ensures planar alignment, i.e. the helix adopts a radial orientation. This leads to omnidirectional selective reflection from the cholesteric droplets giving rise to peculiar and attractive optical phenomena. We demonstrate the specific way of photonic cross communication between droplets, resulting in multicolored and symmetric patterns. Apart from being fascinating from a fundamental optics perspective, the system holds extensive potential for applications, e.g. in sensors or in anti-counterfeiting tags.

Cellulose nanocrystal (CNC) is a novel bionanomaterial that currently attracts considerable international attention. It is produced from natural cellulose sources by extracting the smallest structural element in the form of crystalline nanorods. At certain concentrations a CNC suspension develops a cholesteric liquid crystal phase with consequent helical modulation of the nanorods. We developed a new method of drying CNC suspensions under controlled shear flow, yielding a thin CNC film with an unusually high degree of structural control. A key element is to delay and slow down the glass formation which competes with liquid crystalline ordering as the CNC concentration is increased when the water evaporates. Films dried under appropriate conditions exhibit large-scale uniform iridescent properties, a result of a uniformly aligned helix with pitch in the submicron scale. By increasing the circular shear flow the helix can however also be unwound and a uniformly birefringent film is produced.

Keywords: cholesteric liquid crystals, colloidal crystals, self-assembly, optical pattern formation, photonic cross communication, cellulose nanocrystals (CNCs), circular polarization

Student Number: 2012-22446

Contents

List of Figures and Table

Figure 3.2. Hexagonally close-packed colloidal crystals of cholesteric droplets, produced from cholesteric liquid crystal mixtures that give strong selective reflection in the blue **(a)**, green **(b)**, and red **(c)**, respectively. In the inset of **(b)**, the right- and left-handed circularly polarized reflectance of a droplet is shown. The disappearance of the central reflection spot for left-handed transmission indicates a right-handed cholesteric helix. The scale bar is 200 μm.

Table 1. Tunability of the cholesteric pitch by changing the chemical ratio of CB15 / RO-TN 615 mixtures.

Figure 3.3. A hexagonally close-packed array of red-reflecting cholesteric droplets, observed in reflection between crossed polarizers. The field aperture is continuously opened, to successively expand the illuminated area **(a-g)**. **(h)** Schematic of the photonic communication between droplets, giving rise to the multicolored pattern.

Figure 3.4. Droplets of about 50 μm in diameter, produced from red-reflecting cholesteric mixture, observed in reflection mode polarized optical microscopy. The lower series show the optical behavior of the central droplet in the upper image, as the field aperture is gradually opened.

Figure 3.5. Schematic of direct (D) photonic communication between nearest neighbor (*nn*) droplet, and the communication mediated via total internal reflection (TIR) against the surface of the continuous phase with nearest neighbor (*nn*) and with next next nearest neighbor (*nnnn*) droplet.

Figure 3.6. Sequence of spot migration, as the droplets move towards the surface of the continuous phase. The wavelength is shifted to shorter values. For visualizing the movement of the *nn*-TIR spots, white arrows of constant length and

constant starting point are inserted in the two panels **(c-d).**

Figure 3.7. Sequence of photos showing the result of decreasing the cholesteric pitch. The cholesteric droplets are arranged into colloidal crystals giving rise to multicolored reflection patterns. As the pitch is decreased the central spot (normal reflection) changes from IR wavelengths **(a)** to green colored reflection **(f).** Scale bars are 100 μm.

Figure 4.1. CNC film texture as a function of circular shear flow during the evaporation; produced from 0.37wt.-% of CNC suspension (fully isotropic state) without shear flow, exhibiting stripe and non-stripe pattern in multi-domains **(a)**, and also starting from a fully isotropic state of suspension with shear flow, that show non-stripe pattern which induced by uniform helix orientation with selective reflection **(b)**.

Figure 4.2. CNC film from isotropic suspension at low concentration of 1.0wt.-%, with shear flow during the evaporation, the helical orientation is more uniform as confirmed by an unchanging color when rotating the sample between crossed polarizers; **(a)** and **(b).** Without shear flow during the process, the helix orientation is not uniform, giving rise to birefringence when rotating the sample; **(c)** and **(d)**.

Figure 4.3. Dried CNC film (4.8wt.-% of CNC starting concentration) produced with non-shear flow **(a)**, and film texture observed between crossed polarizers **(b).** Inserting λ/4 plate, the left-handed circular polarization is confirmed through left-handed analyzer **(c),** also not passing through right-handed analyzer **(d).**

Figure 4.4. CNC film from liquid crystalline starting suspension at a high concentration of 4.8wt.-%. A strong shear flow induces unwinding of helix during the evaporation, removing the selective reflection. The film is observed in

1. Introduction

1.1 Motivation and Goals

A recent demonstration by Humar and Musevic of omnidirectional mirror-less lasers from small droplets of dye-doped cholesteric liquid crystal [1] created much interest in the photonics community. The inherent helical structure of a cholesteric liquid crystal provides a photonic band gap resulting in strong selective reflection of a narrow wavelength regime [2], allowing for mirrorless lasing upon doping the droplets with a dye. Since the droplets have spherical symmetry it leads to the lasing in all directions, yielding a 3D omnidirectional laser. Humar and Musevic used a simple approach to prepare an emulsion of cholesteric droplets by stirring the liquid crystals in excess glycerol. Problems with this approach are the polydispersity of droplets and the lack of stabilization of the droplet interface with the continuous phase. As a possible means forward to large scale application, we here demonstrate the production of monodisperse liquid crystal emulsions with uniformity and high speed production using a nested capillary microfluidic approach. Moreover, a water soluble polymer is introduced as a stabilizer for achieving long term stability of the droplets, and also for ensuring the desired planar surface anchoring of the director in the droplets. Investigations of the monodisperse emulsions produced with the improved method additionally revealed interesting and peculiar optical phenomena. When the uniform droplets are self-assembled into 2-dimensional colloidal crystal arrangements, multicolored and symmetric patterns arise. We could successfully explain the origin of these patterns and demonstrate how they can be tuned.

Cellulose nanocrystals (CNCs) constitue an attractive renewable nanomaterial, with suspensions of CNC exhibiting a liquid crystalline phase over a certain range of concentration. Since the liquid crystalline behavior of CNCs was introduced, it was proved that the CNC suspension develops a cholesteric phase with left-handed helical structure and selective reflection was observed from dried films.. However, the detailed mechanisms of the helix formation process in the aqueous solution and of pitch variation dependent on concentration have not yet been studied. The end of the thesis describes the first part of an on-going study aimed at filling this gap. We produce thin films from CNC suspensions with varying starting concentration. Moreover, by developing a new method of drying films under rotating shear flow we can unify the helix orientation into an overall vertical direction, giving advantages for potential applications of CNC films.

2. Research background for this work

2.1 Liquid Crystals

The word *phase* is used as a term describing state of matter. One commonly categorizes matter into three phases which are crystalline solid, liquid and gas phases. A solid crystal has a rigidity reflecting that the atoms are tightly located with respect to each other with long-range positional order. In contrast, liquid and gas are fluids. The molecules are relatively free to move without long-range order. We may call this an isotropic state, meaning that it behaves uniformly in all directions. Between crystalline solid and liquid states there are—for some substances—liquid crystals that share properties of the two surrounding phases. The uniqueness of liquid crystals is that they are anisotropic fluids with long-range orientational order. Their intermediate character gives them the name *mesomorphic states* or *mesophases* and constituents forming liquid crystal phases are called *mesogens*. The structural shapes of mesogens are anisotropic, that is, they are rod-like (sometimes called calamitic), disc-like (or discotic) or more complex, like banana-shaped.

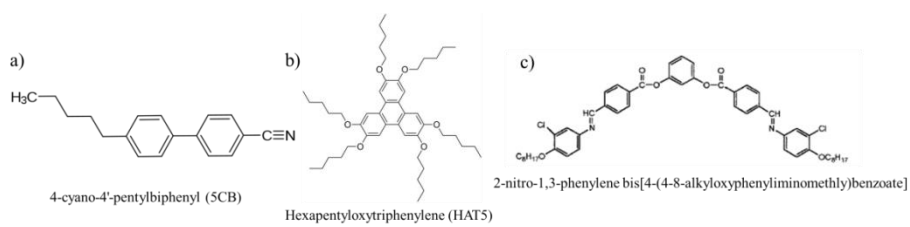

Figure 1.1. Examples of liquid crystal molecules for (a) calamitic, (b) discotic, and (c) banana shaped anisotropy.

The origin of liquid crystals was that, in 1888, the Prague scientist Friedrich Reinitzer observed that cholesterol benzoate has double melting points. That was the first discovery of liquid crystal. After that the German scientist Otto Lehmann investigated Reinitzer`s sample with a polarizing optical microscope and established the concept of *flowing crystal* with the intriguing optical property birefringence.

The liquid crystalline systems are mainly classified as thermotropic and lyotropic liquid crystals. Thermotropic liquid crystals are made up of individual molecules that order in a liquid crystalline fashion. Phase transitions of thermotropics are driven by temperature. The two fundamental parameters of temperature are melting point T_m, indicating the beginning of the liquid crystalline phase on heating from the crystalline solid, and the clearing point T_c into an isotropic liquid. [3]

Liquid crystal phases can be categorized by the degree of molecular order. The orientational order can be quantified by the *order parameter* $S = \frac{3}{2}\left\langle \cos^2 \beta - 1 \right\rangle$, an average describing the fluctuations by an angle β of the molecules away from the preferred direction, denoted the *director* **n**. The practical value span of the order parameter is between 0 and 1, with a perfect crystalline solid having $S = 1$ ($\beta = 0$ for all molecules) and an isotropic liquid having $S = 0$.

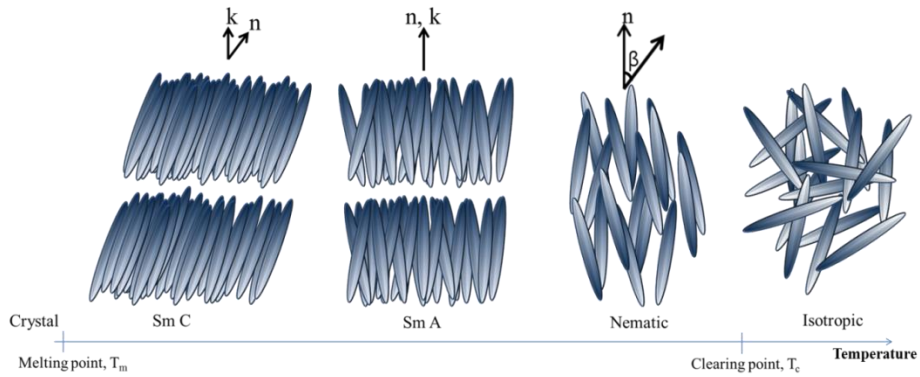

Figure 1.2. Schematic of phase sequence of common thermotropic liquid crystals. The vector **k** means the smectic layer normal, and the angle **β** describes the molecular fluctuations with respect to the director **n** (a sign-invariant vector).

The nematic phase is the simplest liquid crystal phase. It has long-range orientational order without positional order. The smectic phases, the SmA and SmC phases being the most important examples, possess a layered structure which indicates a one-dimensional (1D) positional order, and we can define a smectic layer normal **k** which can be along **n** (SmA) or at a certain angle from **n** (SmC).

The double faced property of liquid crystal phases can from a chemical structure point of view be assumed be related to an analogously dual character on the molecular scale. In the case of thermotropics each molecule combines a rigid part (often a core of two or more aromatic rings) with one or several flexible moieties (typically aliphatic chains). In lyotropics the solvent (the ”continuous phase” in colloid terminology) provides the flexibility, whereas the rigidity (or semi-ridigity) is given by the suspended ”nano objects” (for instance nanorods, nanodiscs or aggregates of amphiphilic molecules that are called ”micelles”)

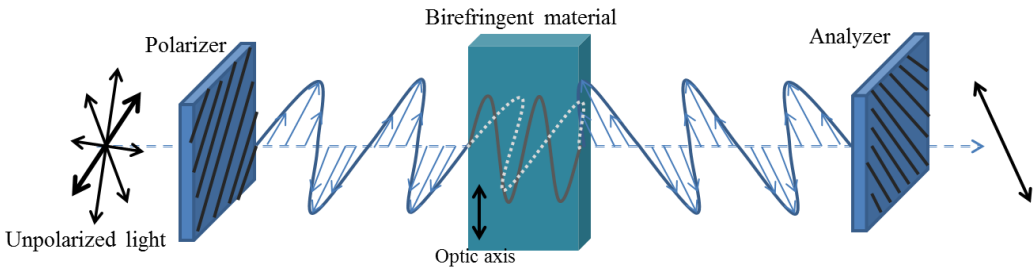

Figure 1.3. Schematic of double refraction in a birefringent system between crossed polarizers. The light oscillates perpendicular to the dashed horizontal line, and inside the birefringent material it splits into an ordinary wave (dotted wave) and an extraordinary wave (continuous wave). The outcome of phase shift, between the two waves, in this figure is $\lambda/2$.

Birefringence is an outstanding optical property of liquid crystals. The fundamental characterization method of liquid crystals for birefringence is polarizing optical microscopy. An alternative name for birefringence is double refraction. It means that there are two refractive indeces *(n)*.

As seen in Fig. 1.3., a sample is placed between two linear polarizers that are crossed 90° in terms of their transmission directions. A source emits unpolarized light, which changes the directions of oscillation randomly, that then goes through the polarizer. The polarizer lets through linear polarized light, i.e. the electric field oscillates in one direction only. When linearly polarized light enters a birefringent medium, the light is split into two waves, and they travel with different velocities. We call them *ordinary wave*, for which the electric field oscillates perpendicular to the optic axis, and *extraordinary wave*, where the electric field oscillates parallel to the optic axis. The ordinary wave experiences the ordinary refractive index (n_o), and the extraordinary wave experiences the extraordinary refractive index (n_e).

Since the magnitude of the refractive index tells how much the light velocity in the medium is reduced, the two waves go through the plate with different velocities. When they come out from the birefringent material, they are recombined but now with a phase shift. If this phase shift results in a change in the polarization state, a portion of light can be transmitted through the analyzer. Otherwise, if the polarization state or direction is not changed by the birefringent material, the outcome will be dark without transmitted light. By subtracting the two refractive indices, the birefringence of the material is defined (1).

$$\Delta n = n_e - n_o \qquad (1)$$

Moreover, we can calculate the magnitude of the phase difference after passing the birefringent object is (2):

$$\Delta\phi = 2\pi\left(\frac{d}{\lambda}\right)\Delta n \qquad (2)$$

where $\boldsymbol{\lambda}$ is the vacuum wavelength of incidence light, and $\boldsymbol{d}$ is the sample thickness. We will introduce the color effect of birefringent materials between crossed polarizers, as a function of sample thickness (μm) and birefringence in Chap. 4.

2.2 Chirality in Liquid Crystals: Cholesteric phase

Cholesteric liquid crystal phases constitute some of the most beautiful examples of liquid crystallinity, as they can exhibit extraordinary photonic phenomena related to a regular internal structure that is periodic on the same scale as visible light wavelengths. More specifically, this periodicity is generated by a helical modulation of the director.

The simplest way, in which one obtains a chiral liquid crystal, is to introduce chiral molecules or particles in an achiral host phase. If the chirality of the dopant is transferred to the phase we call this an *induced chiral system.* In our work on thermotropic liquid crystals we used this approach, whereas in our work on cellulose nanocrystals the mesogens themselves (the cellulose nanorods) are chiral. Chirality in liquid crystals is generally indicated by an asterisk (*) and the cholesteric phase can thus be abbreviated N*, referring to it being a chiral version of the nematic phase.

The helix periodicity is obtained by a full turn of molecular director. It is often called the pitch *p*, and the length ranges from a few hundred nanometers to infinity. In a nematic liquid crystal the states of inversed director, n and $-n$, are indistinguishable. The result is that the periodicity of physical properties, e.g. optical properties, is half the pitch $(p/2)$. For light incident along the helix axis, the optical response of a cholesteric phase has three different regimes depending on the period of the helix. If helical pitch is much longer than visible wavelengths $(p>\lambda)$, the polarization direction of light rotates following the rotation of the director. This is sometimes called the wave-guiding regime, or Mauguin mode, after the French physicist who first described this behavior. But if the pitch is in the order of λ $(p \sim \lambda)$, and if it is circularly polarized with the same handedness as the cholesteric helix,

the light is selectively reflected. If the incident light is unpolarized or linearly polarized, it is split into two circularly polarized components, one left- and one right-handed.The component with the same handedness as the helical structure of the cholesteric is fully reflected, while the other one is fully transmitted. Thus, as a consequence of a left-handed cholesteric helix, the selectively reflected light is left-handed circular polarized. When the helix pitch is much shorter than the wavelength ($p \ll \lambda$, *or for* visible wavelengths, $p < 300nm$), all light can be transmitted, and the polarization plane of linearly polarized light is rotated in a similar way to other optically active media (e.g. quartz).

The selective reflection phenomenon of cholesterics can be quantitatively described through Bragg`s relation:

$$n\lambda = 2d\sin\theta \qquad (3)$$

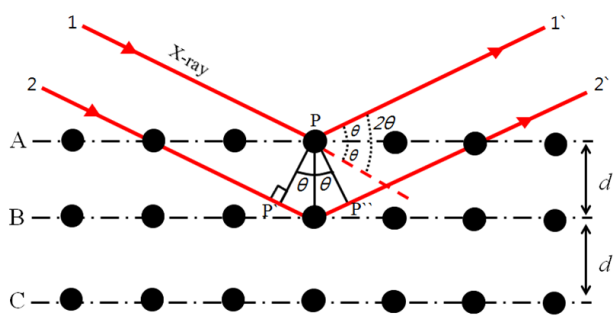

Figure 2.1 Schematic of the diffraction of x-ray from crystals, demonstrated by Bragg's law.

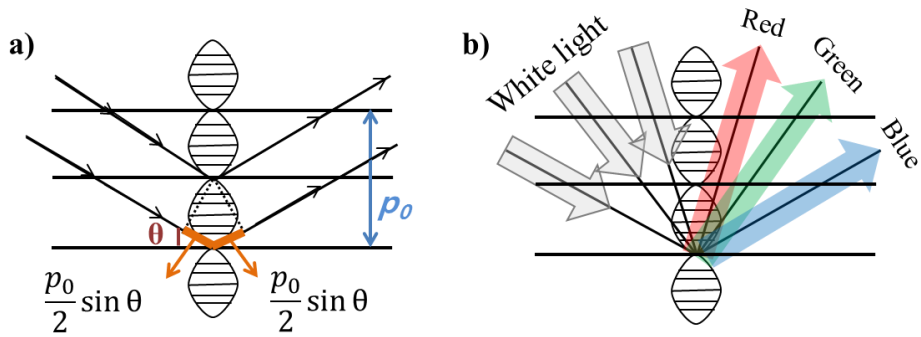

Figure 2.2. Schematic of selective reflection in cholesterics, according to the pitch ***p***. A decrease of angle θ leads to a decrease of the wavelength of the selected transmitted light.

where *n* is an integer, λ is the wavelength of the incident light, *d* is the periodicity of the medium and α is the angle of incidence, as defined in Figure 2.1. In 1912, W. L. Bragg introduced this relation for describing the diffraction of x-rays from crystals [4]. Following his explanation, the light reflected at different crystal planes (separated by a constant distance *d*) interferes constructively when the phase shift between reflected beams is equal to 2π.

In cholesterics, Bragg's relation applies after *d* is replaced by the optical periodicity *p*/2, thus:

$$n\lambda = p\sin\theta \qquad (4)$$

Since *p* is on the order of visible light wavelengths the selective reflection occurs for visible light, giving rise to the iridescent color characteristic of cholesterics. As indicated by Equation (4) the color depends on the helix pitch *p* but also on the

angle of incidence.

Because the optical properties of cholesterics depend strongly on how the helix is oriented with respect to the direction of incident light, it is important to be able to control the alignment of the director, and thus of the helix. This is often achieved by bringing the liquid crystal in contact with surfaces that have been treated to induce the desired molecular arrangement. For selective reflection we want the helix orientation to be close to the direction of light propagation, thus generally perpendicular to the sample plane. Since the helix is perpendicular to the direction, this is achieved by planar surface treatment, that is, the director **n** is in the plane of the sample (see Figure 2.3). A flat cholesteric sample then shows a uniform reflected color, often interrupted by so-called ”oily-streak” defects, caused by local misorientations of the helix.

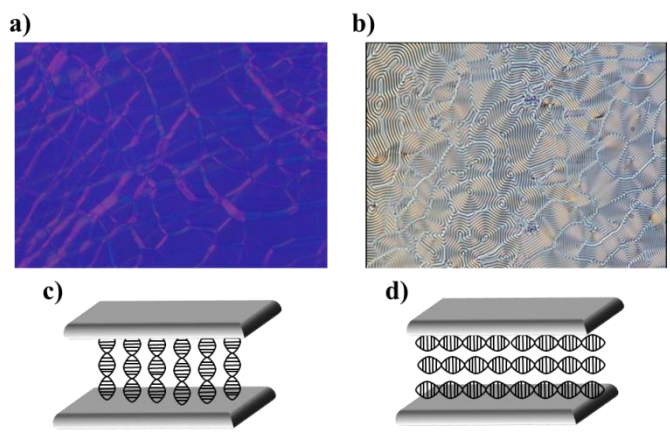

Figure 2.3. Textures of the cholesteric phase according to the surface treatments when the direction of incident light is perpendicular to the surface. The “oily-streak” defects with uniform reflected color **(a)** correspond to the regime of **(c);** helix axis is vertical to the surface (planar anchoring). The fingerprint texture **(b)** is induced by parallel direction of helix axis to the surface (homeotropic alignment) **(d)**.

In contrast, when the surfaces are treated to induce perpendicular alignment of the director **n** (often referred to as ”homeotropic” alignment), this leads to a helix axis that runs parallel to the surface. If the pitch is longer than light wavelengths this is recognized in the polarizing microscope as a finger-print texture, because the periodically changing angle of the molecules with respect to the light polarization leads to a periodic modulation of the effective birefringence, and thus of the light intensity between crossed polarizers, cf. Figure 2.3.

2.3 Cellulose Nanocrystals (CNCs)

Cellulose is one of the natural polymers that is considered as a key source of sustainable materials. Recently government and industry are increasingly demanding products made from sustainable and renewable resources, and cellulose-based materials thus attract much attention because they are carbon neutral, biodegradable, and environmental animal/human health and safety risks are low. For centuries cellulose has been extracted from wood or cotton, to be used in wood, paper and textiles, but today new means of processing cellulose are being developed [5-6].

Cellulose is an organic compound with the formula $(C_6H_{10}O_5)_n$, a polysaccharide consisting of a linear chain of several hundred to over ten thousand glucose units. The inter-chain hydrogen bonding, between hydroxyl groups of one chain and oxygens of nearby chains, stabilizes the structure and results in the linear configuration of the cellulose chain. It means that the inter-chain network of hydrogen bonding makes cellulose a mechanically stable polymer, and gives cellulose fibrils high axial stiffness. Such cellulose fibrils provide an important reinforcing function for algae, plants etc [7-8].

Cellulose fibrils have two main regions, where one is highly ordered crystalline and the other is a slightly disordered amorphous region. Removing the amorphous part of cellulose microfibrils by acid hydrolysis, we can extract *cellulose nanocrystals (CNCs)*. Cellulose nanocrystals are rod-like and whisker-shaped nanoparticles, with a high aspect ratio (5-10 nm wide, about 100 nm in length). In the acidic hydrolytic reaction, a strong acid such as hydrochloric or sulfuric acid is normally used. For the materials used in our work sulfuric acid was used. During the controlled sulfuric acid hydrolysis, sulfate ester groups are attached to the

surface of the cellulose nanocrystals, leading to a high surface charge from functional groups that allow a stable dispersion in water. Through this process we could achieve a CNC suspension with pH ≈ 4.

Since the CNCs are chiral, the CNC suspension forms a chiral nematic phase at a few weight percent concentrations. This means that the rods organize with local uniform orientational order, aligning along a common director **n**, but the director orientation is helically modulated along a direction perpendicular to **n**. Since the helix formation is induced by the chirality of the cellulose, the helix pitch decreases when the CNC concentration increases. If the concentration gets high enough the pitch can reach the realm of visible light wavelengths and thus also films produced from CNC suspensions can show beautiful iridescence.

3. Cholesteric liquid crystal droplets produced by microfluidics

3.1 Used materials

The cholesteric (N*) liquid crystal mixtures were composed of the commercial nematic liquid crystal mixture RO-TN 615 from Roche (Switzerland) and the chiral dopant (S)-4-Cyano-4'-(2-methylbutyl)biphenyl (CB15), purchased from Synthon Chemicals (Germany). The host mixture (RO-TN 615) actually already contains a small amount of chiral dopant (cholesterol nonanoate), intended to promote a single handedness of twist when the mixture is used in a display device of Twisted Nematic (TN) type, and it is thus already chiral. The original quantity of cholesterol nonanoate is however so low (<1%) that no helix formation can be detected. By adding CB15 at high concentration (several tens of percent) we induce a much stronger phase chirality, giving rise to a helix pitch that can be as small as visible light wavelengths. The helix pitch in the mixtures can be tuned to reflect from the infrared to the ultraviolet range, with visible normal-incidence reflection from CB15 concentrations between 30 wt.-% to 50 wt.-%.

For ensuring planar alignment, i.e. **n** in the plane of the interface between droplet and continuous phase, and counteracting coalescence of the liquid crystal droplets in aqueous solution, they were dispersed in a continuous phase consisting of a distilled water + glycerol mixture (50/50 volume ratio) in which 3 wt.-% polyvinylalcohol (PVA) was dissolved (from Sigma-Aldrich, M_w = 31,000 – 50,000g mol^{-1}, 98-99% hydrolyzed).

3.2 Microfluidic Technique

Microfluidic techniques provide a means of controlled flowing of relatively small volumes of liquids through thin channels, with different liquids meeting under well-defined conditions at desired locations. This enables, for instance, the production of monodisperse drops or multi-layered shells [9-13]. Many materials can be used for microfluidic systems, including hard materials like glass, silicon chips or stainless steel. However, the large-scale break-through came with the event of soft lithography, where a chip with embossed channels is made from a soft elastomer like polydimethylsiloxane (PDMS). This technique was pioneered by G. Whitesides at Harvard [14] and it has developed to microanalytical systems, together with numerous methods of fabrication. The analytical device plays a role in a tool, important in biological and chemical analysis. Currently it is also considered as an exquisite way to make an emulsion, flowing multiple immiscible fluids at a time.

The system in our work is slightly different from the standard chip-based microfluidics. We use a capillary microfluidic set-up fabricated by nesting glass capillaries with square and circular cross sections, with side lengths and diameters adapted to each other. This approach follows the design of Utada et al [15]. Among the advantages of this system are the concentric geometry, making it easy to produce spherically symmetric droplets or shells, the ease in tuning droplet size by changing the orifice size and the resistance to organic solvents, in contrast to PDMS. Moreover, the drop formation process can be conveniently observed since the set-up was built by transparent glass capillaries.

When producing liquid crystal droplets, the liquid crystal material is flow-focused into a collection capillary by the outer fluid, flowing in the same outer

channel as the liquid crystal but in the opposite direction, cf. Figure 3.1.The figure shows that the liquid crystal is injected surrounding a tapered cylindrical capillary, inserted coaxially inside the square capillary in which the flow focusing takes place. This inner capillary was added in order to be able to introduce a third fluid inside the liquid crystal, thus turning the droplet into a shell [16-20]. This option was however not used for the work described in this thesis.

As mentioned above, the water-soluble polymer PVA was dissolved in the outer fluid for ensuring a planar anchoring of the director at the droplet-continuous phase interface and also to act as an emulsion stabilizer. The droplet production was done at room temperature, at which the cholesteric mixture is in the liquid crystalline phase. It turns out that the resulting shear flow gives a positive effect on the director alignment: the internal circular flow within the droplet, induced by a continuous phase moving at higher speed than the droplet, favors a director orientation in the plane of the interface, and thus with a radial helix, which is the geometry we need.

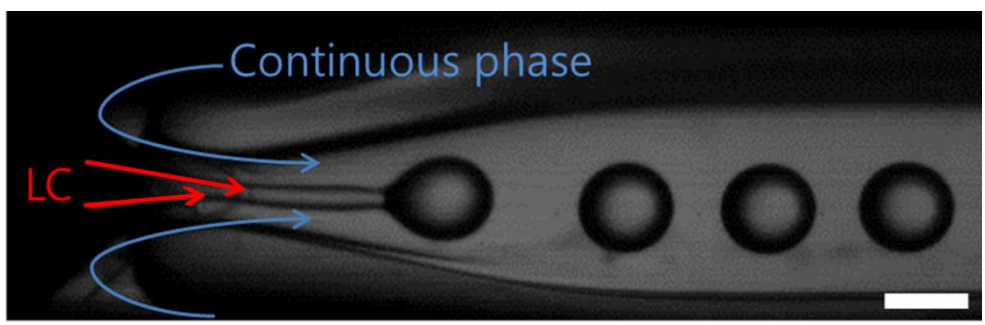

Figure 3.1. Flow-focusing regime for producing liquid crystal droplets by a coaxial microfluidic set-up. Scale bar is 300 μm.

When two immiscible fluids flow coaxially in direct contact with each other, a cylindrical shape of the interface is unstable. This is because the cylindrical interface has a larger surface-to-volume ratio than a sequence of droplets with the same volume, and surface tension thus drives break-up of the cylindrical flow into droplets via a hydrodynamic instability called the Plateau-Rayleigh instability.

The cholesteric stream thus pinches off into droplets soon after the flow focusing. In the appropriate flow conditions, a highly uniform array of droplets can be obtained. The flow rate of the outer phase is generally 2.7 times higher than that of the liquid crystal in our system.

3.3 Sample preparation

After producing the cholesteric liquid crystal droplets in the nested capillary microfluidic set-up, the droplets were collected in a flat container at high volume fraction. Since the density of the liquid crystal mixture is lower than that of the continuous phase, the cholesteric droplets move towards the surface of continuous phase and spontaneously organize into a 2D colloidal crystal arrangement. A silicon chip was generally used as a substrate for the sample observation by polarizing optical microscope, since its opaqueness prevents undesired multiple reflections, which would be the result if a transparent glass slide had been used (top and bottom slide surfaces as well as any surface below the glass slide that the light may encounter). The silicon chips are washed by four steps, dipping in detergent, acetone, isopropanol and deionized water. Each step is conducted for five minutes in ultra-sonication bath. After the whole process, the silicon chip was dried by blowing air.

3.4 Reflection Phenomena observed by Polarizing Optical Microscope

Cholesteric liquid crystal droplets are self-assembled spherically symmetric photonic crystals. When such droplets organize into hexagonally close-packed colloidal crystal arrangements, multiple photonic cross communication modes develop between droplets, resulting in colorful patterns of circularly polarized and strongly reflected spots. The individual patterns can be turned on or off one by one by adjusting the illuminating area. Together with tunability of the cholesteric pitch (which is at the origin of the multicolored patterns) by temperature, chemical composition or confinement, the unique optical properties hold substantial potential for applications [21-25].

We first produced monodisperse cholesteric droplets from cholesteric liquid crystal mixtures that reflect in visible range, with blue, green and red normal reflection color, respectively (Figure 3.1). The cholesteric pitch was tuned by changing the chemical composition in the mixtures. As indicated in Table 1, the higher the concentration of chiral dopant, the shorter is the induced cholesteric pitch *p*, thus reflecting shorter wavelengths of light according to Bragg's relation (Equation (2)). By planar anchoring of the director at the droplet-continuous phase interface, and thus radial helix orientation, the cholesteric droplets exhibit omnidirectional selective reflection, yielding a strong reflective spot at the center of droplet through normal-incidence reflection. This spot exhibits the same color as a flat sample of the same liquid crystal, thus blue, green and red in panes a, b and c of Figure 3.1, respectively. The cholesteric helix handedness is confirmed by inserting a $\lambda/4$ plate into the microscope, creating a phase shift that turns circularly polarized light into linear polarized light and vice versa, the orientation of the

analyzer with respect to the optic axis of the λ/4 plate determining whether right- or left-handed light is transmitted. The central spot in a green-reflecting droplet is observed when the analyzer is set for right-handed circular transmission (inset in Figure 3.1b), indicating that the helix is right-handed.

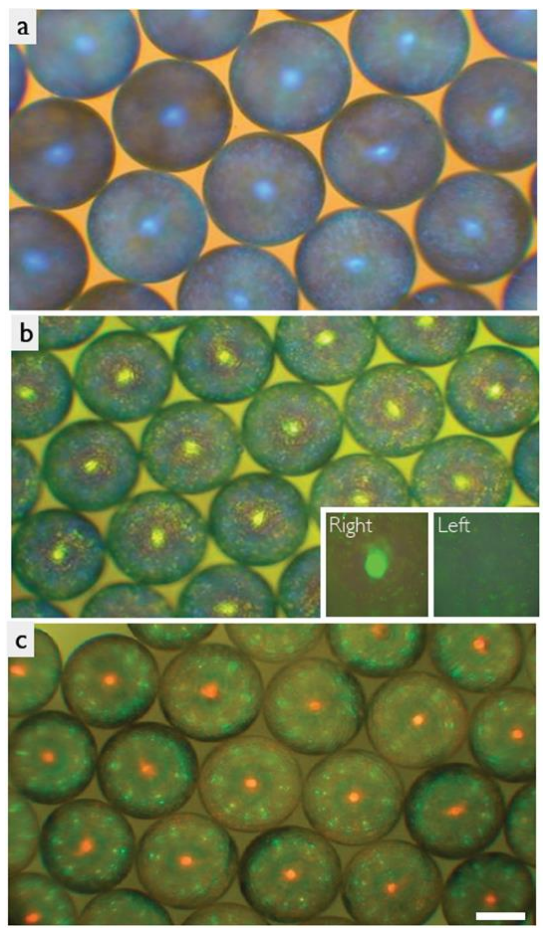

Figure 3.2. Hexagonally close-packed colloidal crystals of cholesteric droplets, produced from cholesteric liquid crystal mixtures that give strong selective reflection in the blue **(a)**, green **(b)**, and red **(c)**, respectively. In the inset of **(b)**, the right- and left-handed circularly polarized reflectance of a droplet is shown. The disappearance of the central reflection spot for left-handed transmission indicates a right-handed cholesteric helix. The scale bar is 200 μm.

Table 1. Tunability of the cholesteric pitch by changing the chemical ratio of CB15 / RO-TN 615 mixtures.

Wt.-% CB15	Normal incidence appearance at room temperature	Normal reflection wavelength, λ
26	**no visible selective reflection**	**826 nm**
28	**no visible selective reflection**	**773 nm**
31	**selective reflection: red**	**702 nm**
33	**selective reflection: red**	**630 nm**
38	**selective reflection: yellow**	**575 nm**
40	**selective reflection: green**	**540 nm**

In red-reflecting cholesteric droplets, we additionally find six-fold symmetric hexagonal patterns in each droplet, consisting of green-blue and green-yellow spots on the periphery (Figure 3.1c). Some spots in the polarizing microscopy image are unclear and even missing which may in part be due to uncontrolled scattering and multiple reflections generated below the droplets. In this early experiment we did not use a silicon chip as substrate but instead a transparent Petri dish. In addition to the added reflections and scattering, later on avoided by keeping the samples on silicon chips, the birefringent plastic of the petri dish also affects the background color.

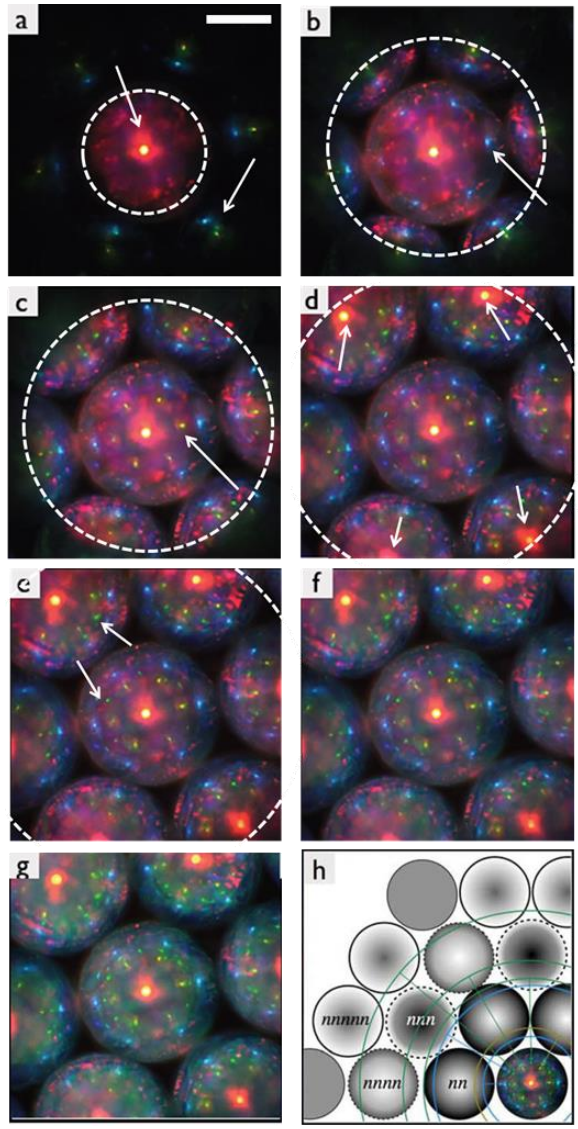

Figure 3.3. A hexagonally close-packed array of red-reflecting cholesteric droplets, observed in reflection between crossed polarizers. The field aperture is continuously opened, to successively expand the illuminated area **(a-g)**. **(h)** Schematic of the photonic communication between droplets, giving rise to the multicolored pattern.

We explored the patterns from red-reflecting cholesteric droplets by changing the illuminating area, using the field aperture of the microscope. If we illuminate the smallest area, as a start, placing the sample such that a droplet in the middle of the colloidal crystal arrangement is at the center, this droplet shows a central selective reflection spot with the fundamental red color (Figure 3.2a). There are also peripheral hexagonally arranged blue and green spots in the surrounding droplets. As will be explained below, the origin of these peripheral spots is the light that is reflected horizontally from the central droplet to the surrounding droplets, which in turn reflect it back up in the vertical direction.

In order to illuminate a large area of the sample, we open the field aperture and blue spots then appear in the central droplet, with six-fold symmetry (Figure 3.2b). The blue spots have the same distance to the droplet perimeter as the blue spots in the surrounding droplets. This phenomenon shows the photonic cross communication between the droplets from the symmetry of peripheral spots. As we continue to open the aperture, also green-yellow spots appear in the central droplet, slightly closer to the center than the blue spots, again with the same distance to the perimeter as the green-yellow spots in the nearest neighbor *(nn)* droplets (Figure 3.2c). This is another confirmation of the photonic cross communication taking place between the droplets.

With a further opening of the aperture, the central red spots appear in the surrounding droplets, and also a new set of blue spots appears in the central droplet, offset by 30° compared to the original pattern (Figure 3.3d). Next, a new set of green spots with the same 30° offset are seen (Figure 3.3.e). The two sets of spots at 30° offset arise from communication between next nearest neighbor (*nnn)* droplets. The aperture is further opened in panes (f) and (g), the final photo

showing the response at full exposure, giving riset o photonic communication between next next nearest neighbor *(nnnn)* and next next next nearest neighbor *(nnnnn*) as well. In pane (h) we describe the central droplet with optically interacting droplets in surroundings. The drawing illustrates that each spot in the central droplet has a corresponding reflection spot in the surrounding droplets. The detailed analysis will follow in the next section.

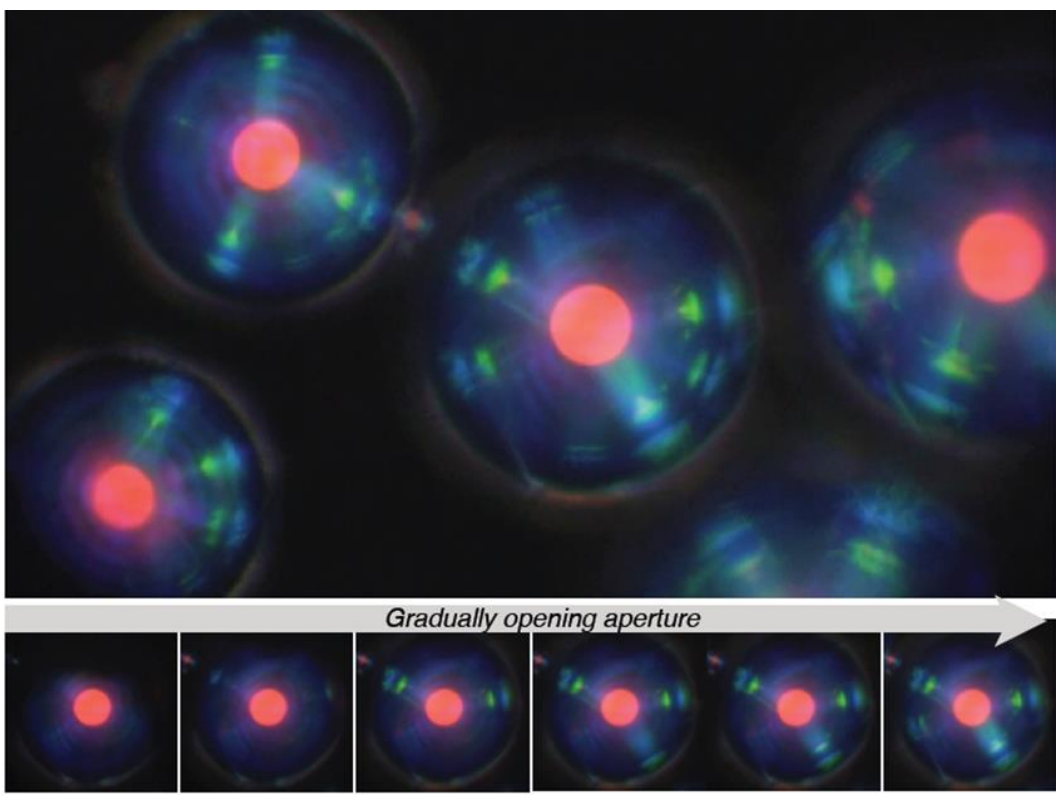

Figure 3.4. Droplets of about 50 μm in diameter, produced from red-reflecting cholesteric mixture, observed in reflection mode polarized optical microscopy. The lower series show the optical behavior of the central droplet in the upper image, as the field aperture is gradually opened.

We also produced smaller droplets of about 50 μm in diameter, observing photonic inter-droplet communication also in this case when the droplets were studied in polarized microscopy (Figure 3.4). In order to achieve accurate analysis with clear spots, a large droplet of about 400 μm in diameter is however optimal. This also makes it easy to bring them into the colloidal crystal arrangements during the collecting process. In smaller droplets, however, the relatively smaller volume fraction of the droplet phase makes it more challenging to organize the droplets into a single-layered colloidal crystal.

3.5 Optical Analysis

We describe the schematic of photonic cross communication between cholesteric droplets (Figure 3.4). The central red spot in each droplet corresponds to normal incidence selective reflection along the helix axis, indicated by the red arrow (0). The blue peripheral spots appear in the central droplet when the vertically illuminated beam (1) is reflected horizontally by an adjacent droplet to the center droplets, i.e. at an angle of incidence $\theta = 45°$. The Bragg equation (2) tells us which is the selectively reflected wavelength at this incidence angle, but it does so in terms of the wavelength inside the liquid crystal:

$$\lambda_{LC} = p \cos \theta \qquad (5)$$

The pitch of this mixture was established to be $p = 420$ nm, using the Cano method (see Appendix. A), and with $\theta = 45°$ we find $\lambda_{LC} = 297$ nm. With an average liquid crystal refractive index $n_{av} = 1.5$ (again established using the Cano method, as described in Appendix A), this translates into an air wavelength of $\lambda_{air} = \lambda_{LC} \cdot n_{av} = 445$ nm. This result matches the observed blue spots, corresponding to what we will from now on call the direct (D) inter-droplet communication.

The first set of green spots appears when growing the illuminated area to encompass ray (2). The ray meets the interface of the adjacent cholesteric droplet at an incidence angle α that is smaller than 45° because ray (2) is closer to the adjacent droplet center than ray (1). The reflected beam with smaller angle is directed to the surface of continuous phase, where it will be totally internally reflected (TIR) because of the higher refractive index compared to the air. The reflection point is exactly middle point between two droplets, and due to the symmetry the TIR beam meets the central droplet at the same angle α. Then by Bragg condition, the same wavelength of light will be vertically reflected, that

leads to the green-yellow spots. We calculated the angle α, using a triangle formed in Fig. 3.4.

$$\tan 2\alpha = b / c = (R - R \sin\alpha) / (R - R \cos\alpha) = (1 - \sin\alpha) / (1 - \cos\alpha) \qquad (6)$$

where the parameters *b*, *c* and *R* are defined in the figure. We solve this equation graphically to obtain that $\alpha \sim 34°$. Using the Bragg relation, we find that the selective reflection should be observed at about 520 nm, fitting with the green-yellow colored spot.

$$\lambda_{air} = n_{av} \cdot \lambda_{LC} = n_{av} p \cos\alpha \qquad (5)$$

$$\Rightarrow \lambda_{air} = 1.5 \cdot 420\text{nm} \cdot \cos 34° \approx 520 \text{ nm}$$

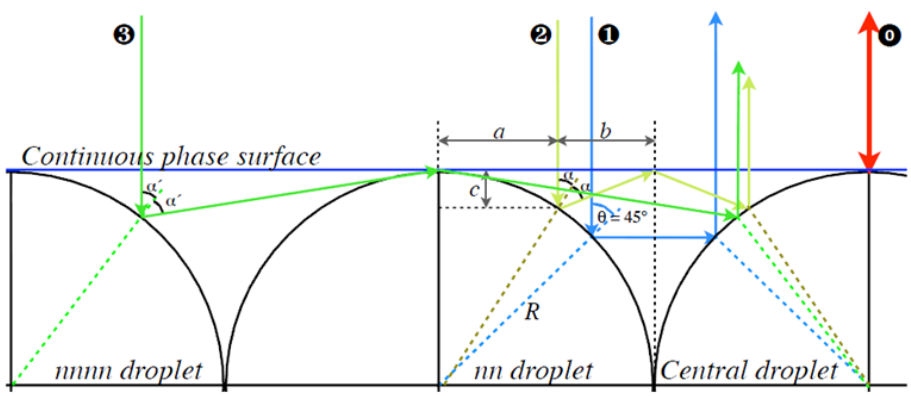

Figure 3.5. Schematic of direct (D) photonic communication between nearest neighbor (*nn*) droplet, and the communication mediated via total internal reflection (TIR) against the surface of the continuous phase with nearest neighbor (*nn*) and with next next nearest neighbor (*nnnn*) droplet.

With a further expansion of the illuminated area, the same sequence of reflection arises with direct (D) and TIR mediated communication involving the *nnn* droplets. Since the array of droplets is hexagonally close-packed, the *nnn* droplet is not in the same vertical plane as the one connecting the central and the *nn* droplets, so we next consider the nnnn droplets for the ray (3) in figure 3.4. After being reflected in the nnnn droplet, also this ray reaches the central droplet via TIR mediated communication. The range is however longer and the angle of incidence α' is correspondingly larger. The Bragg relation then tells us that the reflected wavelength decreases, i.e. it exhibits a blue-shift. As seeing Fig. 3.2, the nnnn spots, appearing with a 30° azimuthal offset from the initial spots, have a more blueish green than the yellow-greennn-TIR spots.

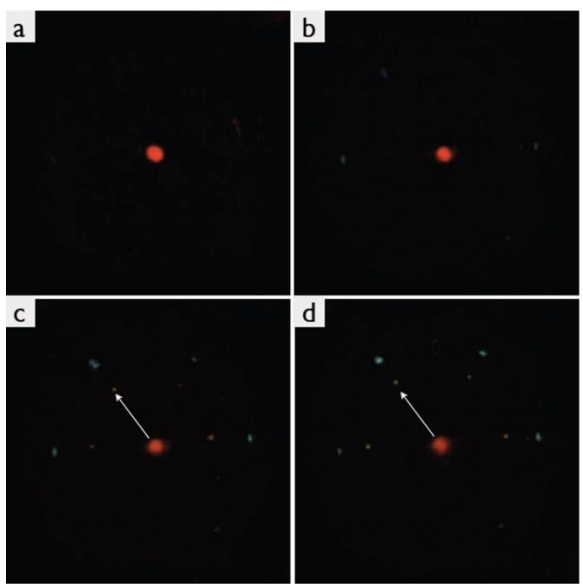

Figure 3.6. Sequence of spot migration, as the droplets move towards the surface of the continuous phase. The wavelength is shifted to shorter values. For visualizing the movement of the *nn*-TIR spots, white arrows of constant length and constant starting point are inserted in the two panels **(c-d)**.

We also investigated the peripheral spots as a function of the distance of the cholesteric droplet from the surface of the continuous phase, focusing particularly on the TIR mediated communication. We added continuous phase onto the array of droplets and followed the reflection pattern (Figure 3.5). Due to the lower density of cholesteric droplets, the droplet array slowly starts to move and float to the raised surface of continuous phase. While pouring the continuous phase, the hexagonal arrangement of droplets in a single horizontal plane was however destroyed slightly, making it difficult to communicate with neighbor droplets. It leads to an initial situation where only the central red spot can be seen in each droplet (Figure 3.5a). While moving towards the top of the system, the hexagonal array is recovered, and it enables blue direct (D) reflection spots to appear near the perimeter (Figure 3.5b). By decreasing the distance to the surface continuously, the *nn*-TIR spots appear which are initially red-shifted and closer to the perimeter (Figure 3.5c), meaning that the reflection angle is smaller than usual in order to reach the longer than usual distance to the surface from the droplet while maintaining the symmetry between adjacent droplets. As the droplets continue to move towards the surface the *nn*-TIR spots move towards the perimeter from the center of droplet. Because the reflection angle increases, the wavelength of Bragg relation decreases, turning the reflected spots more greenish in color (Figure 3.5d). It indicates that the change in wavelength and position reflects the variation of reflection angle at the cholesteric droplet interface.

By varying the helix pitch, the multicolored pattern can be tuned, reflecting the fact that all spots depend on p through the Bragg relation (4). To explore this we simply use different compositions of the cholesteric mixtures. If we increase the pitch to 550 nm, the selective reflection of the central spot is at 825 nm (= 550·1.5),

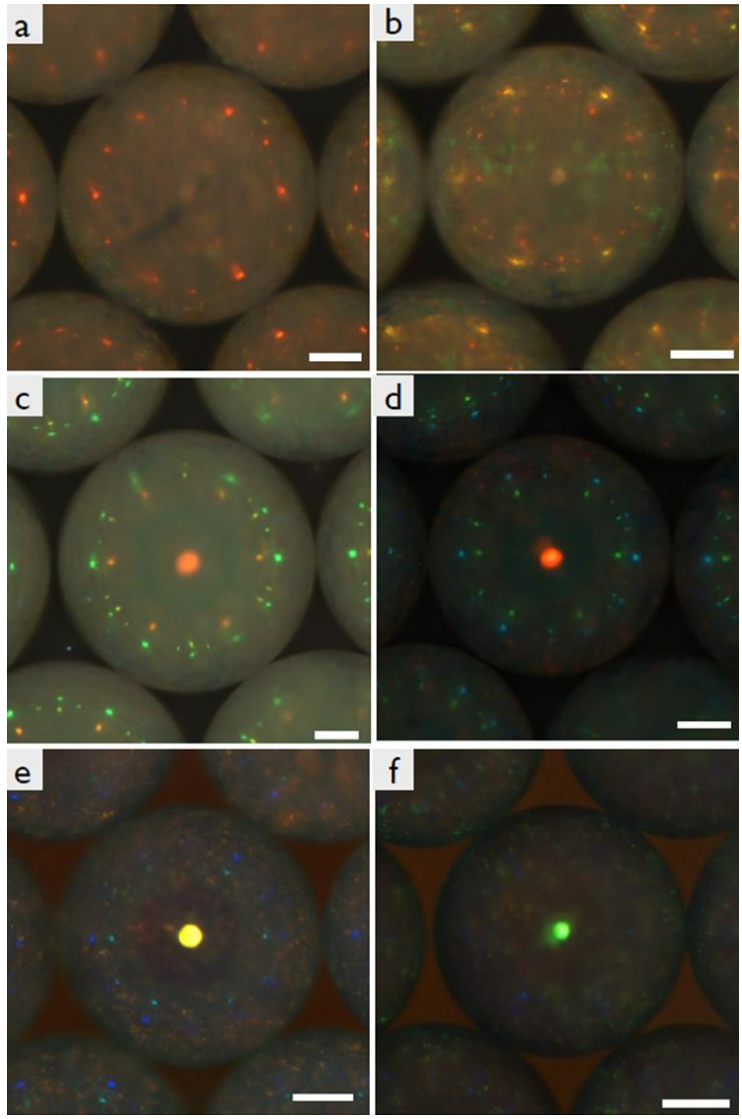

Figure 3.7. Sequence of photos showing the result of decreasing the cholesteric pitch. The cholesteric droplets are arranged into colloidal crystals giving rise to multicolored reflection patterns. As the pitch is decreased the central spot (normal reflection) changes from IR wavelengths (a) to green colored reflection (f). Scale bars are 100 μm.

i.e. in the infrared range. Then the central spot will not be visible, but the outermost peripheral spots are in the visible range, because their reflection wavelength is given by $\lambda_{air} = 1.5 \cdot 550 \cdot \cos 45° = 585$ nm (Figure 3.6a). The *nn*-TIR spots are also not visible because the wavelength is on the border of undetectable region ($\lambda_{air} = 1.5 \cdot 550 \cdot \cos 34° = 685$ nm). By preparing slightly shorter pitch droplets, the *nn*-TIR spots start appearing as orange-red spots (Figure 3.6b). In the panel f, the pitch is reduced to 360nm, and the central spot reflects at 540 nm with green-yellow light. Also the *nn*-TIR spots are detectable at 447 nm with a deep violet color, but the direct (D) spots are now invisible since they are in the UV range. In the end, gradually increasing the amount of chiral dopant, we achieved a series of visible spectra in reflection (a-f).

4. Controlled helix orientation in dried cellulose nanocrystal films

4.1 Used Materials

This research was done in collaboration with Stockholm University in Sweden. The cellulose nanocrystal (CNC) suspension was prepared by the Swedish collaborator. It consisted of CNC with anionic surface charge, originating in sulfate ester surface groups. We focused on three different concentrations of CNC, with different phase behavior; isotropic at 1.0 wt.-%, biphasic at 3.5 wt.-% and fully liquid crystalline at 5.0 wt.-%.

The suspensions were deposited on glass cover slips of 25 mm in diameter, used as a substrate for preparing dry films by evaporating the solvent (water). We patterned a polydimethylsiloxane (PDMS) mold with an identical glass substrate, placing the substrate for the CNC suspension in the mold. In this way we could avoid spreading of the suspension outside the substrate, even when applying a circular shear flow (described in detail below) during the evaporation.

4.2 Film Preparation

In order to influence the orientation of helix formation of CNCs in the film, we developed a new method for drying the CNC suspension. We produce two types of film, dried under circular shear flow and without shear flow, respectively. With the controlled shear flow, we improved the structural control of helix orientation or, at sufficient shear rate, the helix could even be unwound.

In preparation for the experiment the glass cover slip is washed in an aqueous detergent solutionin ultra-sonication bath for 20 minutes. The concentration of detergent solution is about 1-2wt.-%, which is diluted from a concentrated cleaning solution. After that we rinsed the cover slip in deionized water for five minutes in ultra-sonication bath, three times. The cleaned and dried substrate is placed on the patterned PDMS mold. We drop 500 μL of a CNC suspension on the substrate, which should be fully covered even without circular shear flow. For drying without shear flow, a fully covered substrate is placed in a clean atmosphere box to avoid impurities falling on the film. The drying process under controlled circular shear flow was obtained by placing the sample on an orbital mixer, kept in a flowbox that circulated clean air above it to avoid contamination by impurities.

4.3 Optical Characterization

With our new method of drying CNC suspensions under controlled circular shear flow, films with improved uniformity in helix orientation and thus more uniform color can be produced. The goal is to have the helix perpendicular to the plane of the thin dry film that is formed by evaporating the water from the CNC suspension. If the helix is in this direction and if the pitch is in the range of a few hundred nanometers, the film shows iridescent colors due to the Bragg reflection (see equation (4)). In the liquid state, the helix pitch of the cholesteric phase of CNC suspensions is always on the order of several microns, but it can be reduced to the required submicron scale during evaporation of the water, thus producing visible Bragg reflection.

We investigated the different CNC films, produced by drying a suspension that is kept still, as well as by drying while the sample is subjected to circular shear flow at varying speed. When the CNC film is formed without shear flow, the film has a characteristic pattern with multiple domains, exhibiting stripe and non-stripe patterns (Figure 4.1a). As discussed in Section 2.2, the optical response of cholesterics depends on the direction of the helix. When the helix axis is parallel to the surface a finger-print texture arises whereas if the helical axis is perpendicular to the surface, it reflects light that is circularly polarized with same handedness as the helix if the Bragg condition is fulfilled, as discussed and demonstrated in Chapter 3.

The multi-domain pattern of Figure 4.1a indicates that it contains different helix arrangements, with some domains (those with stripes) having a horizontal helix orientation. Also in samples dried with circular shear flow a multi-domain pattern often develops, as in Figure 4.1b, but no stripes are now visible. This important

difference indicates that the helix is now more or less perpendicular to the film throughout the sample, as desired.

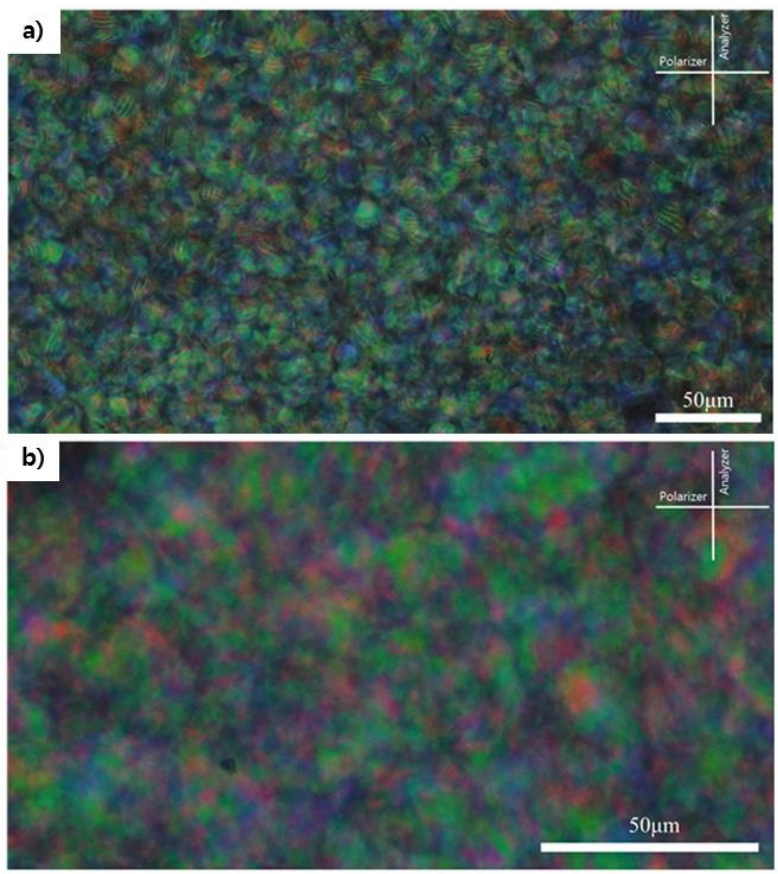

Figure 4.1. CNC film texture as a function of circular shear flow during the evaporation; produced from 0.37wt.-% of CNC suspension (fully isotropic state) without shear flow**,** exhibiting stripe and non-stripe pattern in multi-domains **(a),** and also starting from a fully isotropic state of suspension with shear flow, that show non-stripe pattern which induced by uniform helix orientation with selective reflection **(b)**.

The process of evaporating the water from the suspension is actually highly complex. The increasing CNC concentration does not only decrease the helix pitch of the cholesteric phase, it could trigger further liquid crystal phase transitions and, most importantly, it always triggers gelation, or glass formation, of the system at some point. The risk for gelation becomes substantial once the CNC concentration has been increased to about 10%. From this point on, the liquid crystalline ordering competes with glass formation. When glass formation occurs, it more or less strongly locks in the existing arrangement of the CNC rods, rendering the final dry state a non-equilibrium one.

The key function of the circular shear flow is that it promotes director alignment in the sample plane, and thereby helix formation perpendicular to the film. Once the gelation occurs the helix can no longer reorient because the system is now in a glassy state, but if the helix has been oriented perpendicular to the film plane prior to gelation, this is acceptable. The pitch can apparently still decrease as the water is evaporated, most likely due to a gradual compression of the structure as the solvent escapes from the system. The change occurring after gelation is thus mainly a quantitative one, leaving the structure qualitatively intact, i.e. with a helix perpendicular to the film plane. Since the pitch finally reaches the desired length of a few hundred nanometers we end up with the iridescent film shown in Figure 4.1b.

The variation in color between domains most likely signifies slightly different CNC concentration for onset of gelation, leaving different amounts of water to yet evaporate and thus a varying degree of compression during the drying process. Blue areas would in this scenario have gelified at lower concentration, giving stronger compression of the helix and thus shorter final pitch than in the red domains, where the CNC concentration may have reached slightly higher level

before gelation, resulting in a slightly lower degree of compression upon evaporation of the water.

We also explore the influence on the helix formation process from variations in the initial concentration of the CNC suspension. Films formed from an initially isotropic suspension, with a low starting concentration of about 1.0wt.-%, under controlled shear flow, show selective reflection and uniform helix orientation, as evidenced by the absence of fingerprint texture and by selective reflection being seen throughout the sample (Figure 4.2a-b).

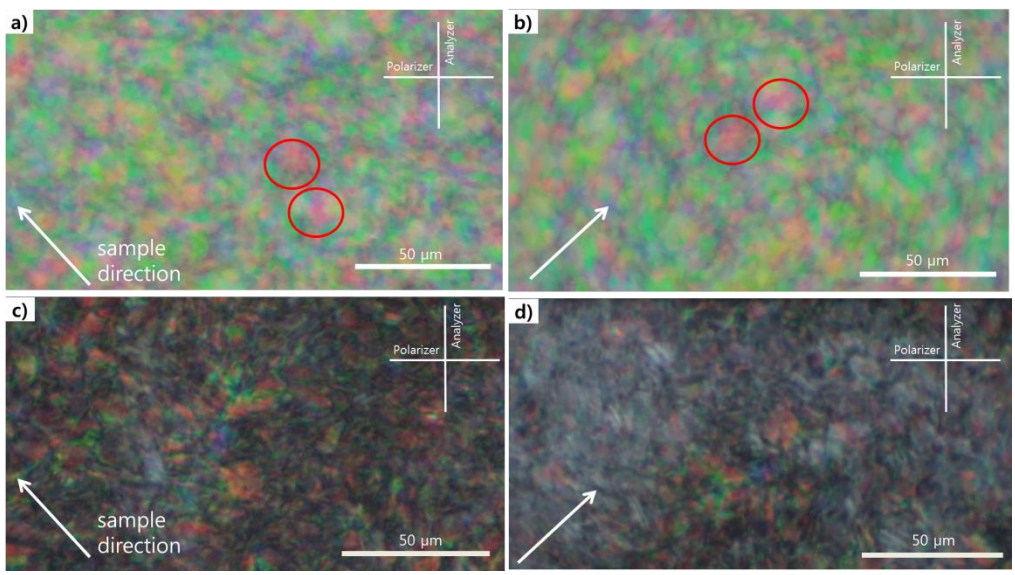

Figure 4.2. CNC film from isotropic suspension at low concentration of 1.0wt.-%, with shear flow during the evaporation, the helical orientation is more uniform as confirmed by an unchanging color when rotating the sample between crossed polarizers; **(a)** and **(b)**. Without shear flow during the process, the helix orientation is not uniform, giving rise to birefringence when rotating the sample; **(c)** and **(d).**

The uniformity of the vertical helix orientation is confirmed by rotating the sample between crossed polarizers, giving rise to almost no change in appearance (see the two encircled locations for clarity). This is expected when viewing a cholesteric along the helix, whereas a cholesteric viewed more or less perpendicular to the helix changes character strongly due to the effect of rotating the optic axis in the sample, which is then strongly birefringent.

In contrast, a film produced without shear flow during the evaporating process, shows a color between crossed polarizers that changes by rotating the sample. This means that the film is birefringent with (at least a projection of) the optic axis in the sample plane, i.e. the helix is not perpendicular to the film.

As we did in Chapter 3 for the thermotropic cholesteric mixture used for producing droplets, we can determine the handedness of the self-assembled helix in CNC films by inspection in reflected light using a circular analyzer (Figure 4.3).

By inserting a λ/4 plate into the microscope, a circularly polarized light beam reflected from the film will experience a phase shift between the linearly polarized components along and perpendicular to the optic axis of the plate, changing the polarization state to linear-polarized. Left- and right-handed circular polarizations yield perpendicular linear polarizations through this process, thus we can determine the handedness by rotating the analyzer and studying at which setting the reflected light is transmitted or blocked.

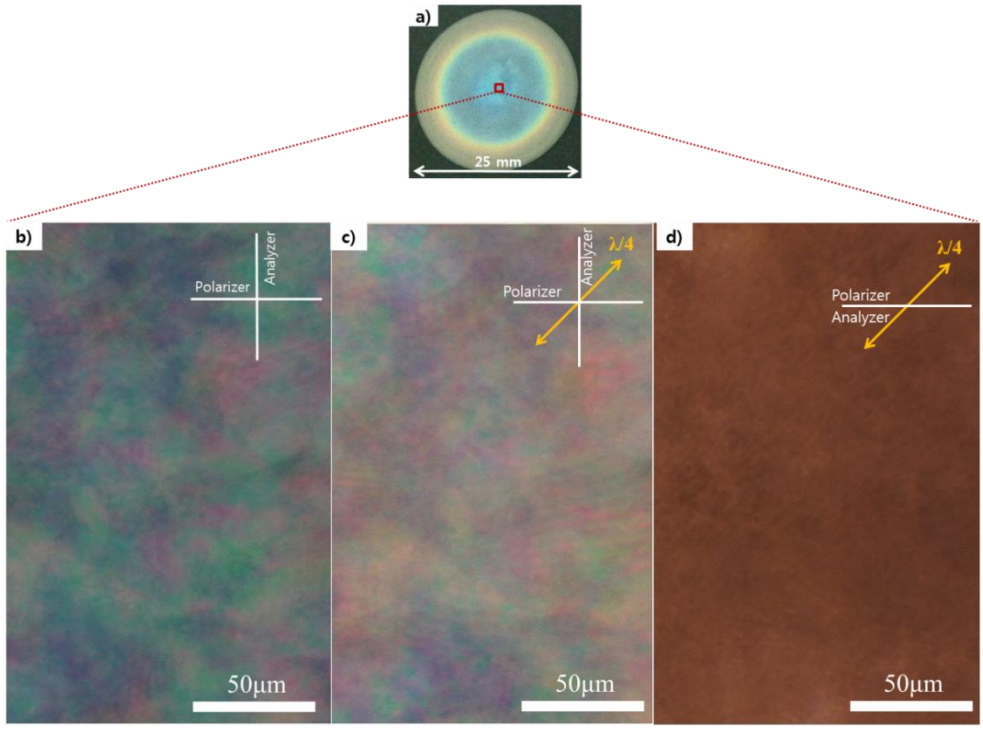

Figure 4.3. Dried CNC film (4.8wt.-% of CNC starting concentration) produced with non-shear flow **(a)**, and film texture observed between crossed polarizers **(b).** Inserting λ/4 plate, the left-handed circular polarization is confirmed through left-handed analyzer **(c),** also not passing through right-handed analyzer **(d).**

Increasing the concentration of CNC suspensions to 4.8wt.-% we achieve a sample that is fully liquid crystalline. When we produced a film from such a suspension under the circular shear flow we found that a strong shear flow removed the selective reflection and instead gave a strongly birefringent sample, thus it was strong enough to unwind the helix entirely. According to Fig. 4.4a, where the CNC film is viewed around the center of rotation during the drying process, the sample is birefringent with a cylindrically symmetric optic axis

orientation. We recall that the intensity I of light transmitted by a birefringent sample placed between crossed polarizers is given by:

$$\mathrm{I} = I_0 \ sin^2 2\theta \ sin^2 \frac{\pi d \Delta n}{\lambda} \qquad (7)$$

where I_0 is the intensity of the incident light, θ is the angle between the optic axis and the polarization axis of the incoming light, d is the sample thickness, Δn is the magnitude of birefringence and λ is the wavelength of the light. In a non-helical nematic-like liquid crystal sample such as this one the optic axis is identical to the director. Equation (7) tells us that if the director is parallel or perpendicular to the axis of the polarizer, light is blocked (the first $\sin^2$ term is zero), yielding a dark appearance in the microscope, regardless of sample thickness and of light wavelength. However, when the director is oriented at an angle of 45 degrees to the polarizer, the highest intensity is achieved. Bearing this in mind we can understand the cross-like texture in Figure 4.4a-b as a result of a cylindrically symmetric director alignment, such that the optic axis is either perpendicular or parallel along a central vertical line as well as long a central horizontal line. When rotating the sample between crossed polarizers, there is no qualitative difference in the texture, confirming the cylindrical symmetry (Fig. 4.4b). However, we still do not know whether we have a radial or a tangential director field, since both these options would give rise to the type of texture seen in Fig. 4.4a-b.

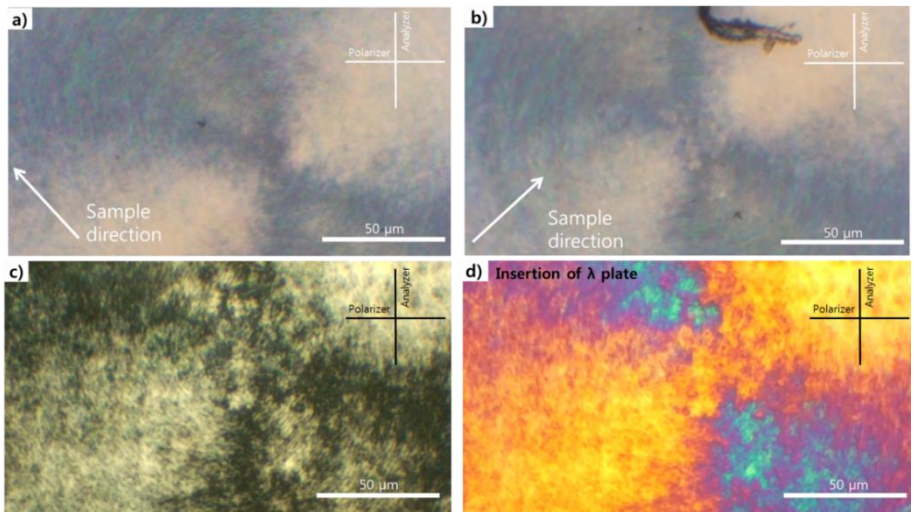

Figure 4.4. CNC film from liquid crystalline starting suspension at a high concentration of 4.8wt.-%. A strong shear flow induces unwinding of helix during the evaporation, removing the selective reflection. The film is observed in reflection **(a-b)**, and in transmission mode **(c-d)**, respectively. By inserting a λ plate, a tangential director alignment is confirmed from the shifts in birefringence **(d)**.

By adding a λ plate, which introduces an optical path length difference of 550 nm (λ for green-yellow light) between the polarization along and perpendicular to its optic axis, we can solve this remaining problem and elucidate whether the director is radial or tangential. Wherever the optic axis of the sample is parallel to that of the wave plate, it adds a phase shift of λ, wherever the two optic axes are perpendicular the effect of the wave plate is to subtract the same phase shift. In Fig. 4.4d, the texture upon insertion of the wave plate with its optic axis oriented between top left and bottom right is shown. The color now changes to blue in the bottom right and upper left corners, but to yellow in the remaning corners. By matching these colors to a Michel Levy diagram (Fig. 4.5) we can understand what is happening.

Initially, before the insertion of the λ plate, the sample is grey-white, indicating that the optical path length difference introduced by the sample is on the order of 100 nm (this can be read off the x-axis of the diagram). If we add 550 nm we end up with a path difference of about 650 nm, which according to the diagram yields blue color. This matches the top left and bottom right quadrants of our texture, suggesting that the director there is parallel to the optic axis of the λ plate, i.e. we would have tangential director alignment. In the remaining quadrants the director should then be perpendicular to the optic axis of the λ plate, and we should have a total optical path difference of 100 – 550 = -450 nm.

The Michel-Levy diagram is not sensitive to the sign of the path difference, that is, -450 nm path difference gives the same color as 450 nm path difference, which we can read off from the chart as being orange-yellow. Indeed, this is the exact color of the bottom left and upper right quadrants of our sample, confirming that we have a tangential director alignment in our CNC film.

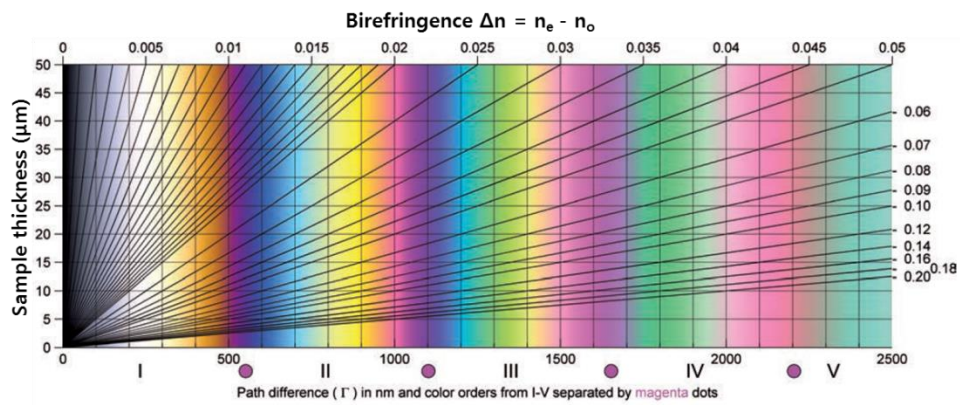

Figure 4.5. The Michel-Levy color chart showing the color of anisotropic materials between crossed polarizers, in terms of sample thickness (μm) and birefringence [26].

4.4 Conclusion

- The advantage of the circular shear flow is that we can simply induce planar director alignment to the sample plane, resulting in vertical helix formation to the film. Another key point is delaying gelation, which can triggers to lock the arrangements of CNC rods to non-equilibrium one. By reducing the risk, films with uniform helix orientation and thus more uniform color are produced.

- When staring at a low concentration of suspension in fully isotropic state, we confirmed the improvement of helix orientation under the appropriate circular shear flow condition.
    - With circular shear flow, film exhibits strong selective reflection, and as evidenced by rotating the sample between crossed polarizers, the uniformity of vertical helix orientation is confirmed, together with uniform texture.
    - Without shear flow, the optical response of the cholesterics shows a different way according to the direction of helix, e.g. multi-domains containing stripe and non-stripe patterns.

- In case of high shear rates and liquid crystalline starting suspension, the helix can be unwound. There is no selective reflection, but it has strong birefringence. By introducing an optical path length difference from a λ plate, the tangential director alignment is confirmed.

Appendix A.

Cano lens method for determining the pitch of a cholesteric liquid crystal

The ‘Cano method’ [you can give reference e.g. to de Gennes & Prost’s ”Physics of Liquid Crystals”] allows one to calculate the helix pitch of a cholesteric liquid crystal based on the texture appearing when confining it between two planar-aligning substrates imposing a specific orientation of the director at each interface (uniform planar anchoring), with a spacing that varies throughout the sample. The classic approach is to use a wedge-shaped sample but a simpler, and in some respects advantagaeous, approach is to place the liquid crystal between a flat substrate and a lens [27]. We used the latter approach in our work.

The uniform planar anchoring boundary conditions first of all ensures that the cholesteric helix runs from substrate to substrate, since the helix axis is perpendicular to the director **n**. Additionally, at each surface **n** must point in the direction imposed by the boundary condition. Since the director field between the surfaces must smoothly mediate between the boundary conditions the helix gets quantized into *half-pitch (p/2)* units. For identical anchoring directions at the top and bottom substrates the spacing α between them must be equal to an integer number *n* of half pitches of the helix, i.e:

$$\alpha = n\,p/2 \qquad (8)$$

If the substrate spacing changes smoothly across the sample, equation (8) is only fulfilled for the natural pitch p_0 in a few locations. In between these locations the pitch must either expand or compress in order to fulfill (8) also at intermediate substrate spacings. If we start at a substrate spacing α equal to $n\,p_0/2$ and let α increase, the liquid crystal will still make n half turns, but of a helix with slightly expanded pitch p_e. Eventually, the distortion away from p_0 will however become smaller if the liquid crystal adds another half turn and compresses the pitch to a value p_c that is slightly smaller than p_0. Every time this happens a defect appears, mediating the n and n+1 regions, and this defect is easily recognized as a line in the polarizing microscopy texture.

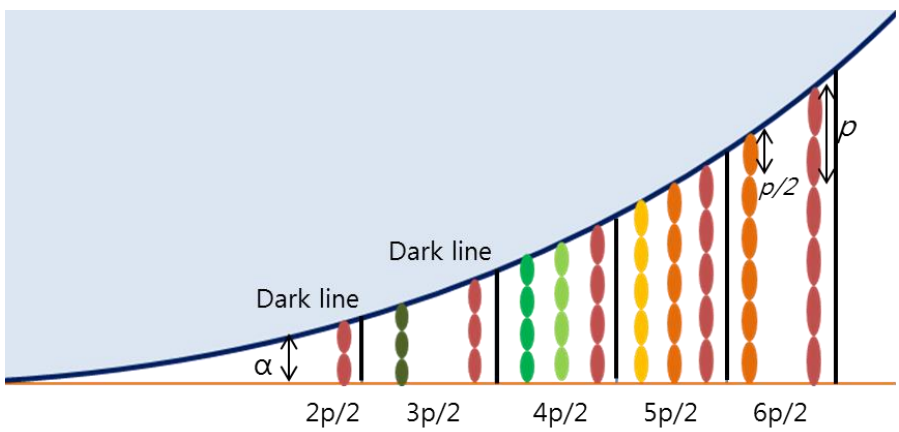

Figure 5.1. Schematic of gradually expanding the helix, quantized into *half-pitch* units (p/2), as the distance between a flat base substrate and a curved top substrate (a lens) increases. Defect lines appear every time a half-pitch unit is added.

The situation is illustrated in Figure 5.1 for the case of a lens on a flat substrate. Going from left to right the helix is expanded by the increasing distance α. This also changes the selectively reflected color of light. The first dark defect line appears when it is favorable to add another half turn with slightly decreased pitch. The color then changes from red-shifted (expanded helix) to blue-shifted (compressed helix), compared to the color of the sample in its natural state, with pitch p_0.

Fig. 5.2 shows the texture obtained in our Cano preparation when a red reflecting liquid crystal was placed between a flat substrate and a lens. Since the helix formation starts at the center with a very short pitch, and since the sample is very thin here, the central circle of is dark and bluish colored, corresponding to short length of pitch. Between two consecutive concentric defect lines the pitch expands and toward the outside it matches the natural pitch, leading to red selective reflection. From the second to fourth lines, the color is changing between adjacent lines from green/green-yellow to red by the gradual expansion of the helix [27].

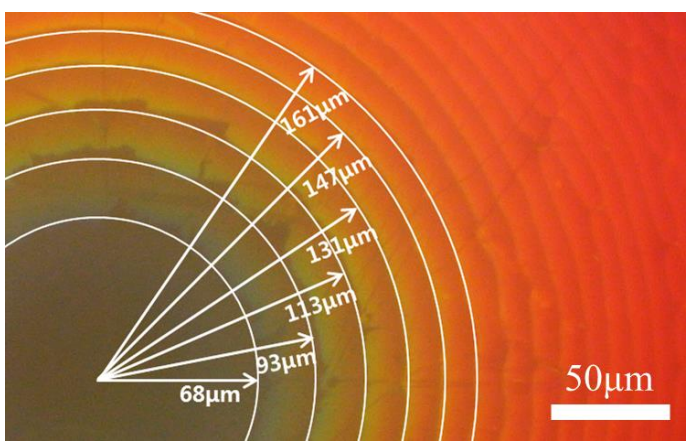

Figure 5.2. Texture of a Cano preparation with a naturally red-reflecting cholesteric liquid crystal mixture. The measured radii of the first few circular defect lines, counted from the center, are indicated.

In order to extract the pitch from the data in Fig. 5.2, we solve the following equation, derived by Pythagoras' law:

$$R_{lens}{}^2 - r_3{}^2 = h_3{}^2$$

and

$$R_{lens}{}^2 - r_2{}^2 = h_2{}^2$$

By subtracting the two heights, it corresponds to the length of half-pitch *p/2*.

$$p/2 = \sqrt{R^2 - r_n{}^2} - \sqrt{R^2 - r_{n+1}{}^2} \qquad (9)$$

The parameter *R* indicates the radius of the lens, which in our case was 10 mm, and the parameters r_n are the radii of the circular defect lines. By calculating the half-pitch *p/2* from interval of defect lines, we obtain the pitch length of about 440 nm for this mixture.

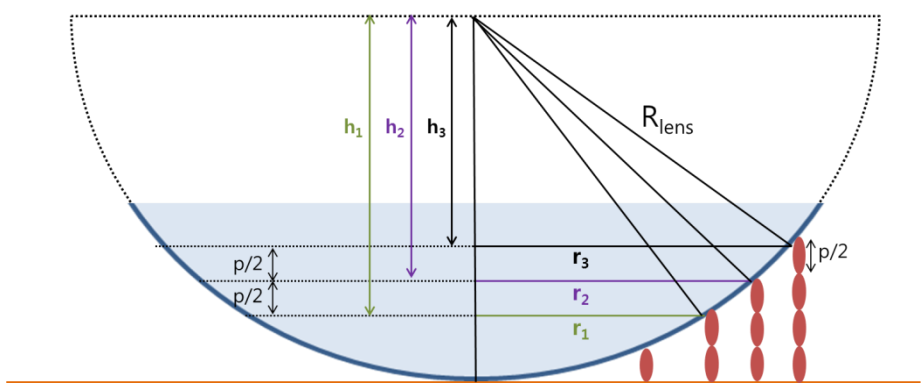

Figure 5.3. Schematic of the Cano lens with the parameters needed to derive the calculation of the cholesteric pitch ***p***.

Finally, by measuring the selective reflection wavelength for normal incidence on a flat sample using a spectrophotometer, we can establish the average refractive index of the mixture, because the reflection wavelength λ, the pitch *p*, and the average refractive index *n*av, are related through:

$$\lambda = n_{av} p \qquad (10)$$

With p = 440 nm and a measured λ = 660 nm, we get an average refractive index of about 1.5.

References

[1] M. Humar, and I. Musevic, *Opt. Express*, 2010, **18**, 26995.

[2] Y. Uchida, Y. Takanishi and J. Yamamoto, *Adv. Mater.*, 2013, **25**, 3234–3237.

[3] J. P. F. Lagerwall, and G. Scalia, *Current Applied Physics*, 2012, **12**, 1387-1412.

[4] P. P. Muhoray, *Nature*, 1998, **391**, 745-746.

[5] D. Klemm, F. Kramer, S. Moritz, T. Lindstrom, M. Ankerfors, D. Gray, A Dorris, *Angew. Chem. Int. Ed.*, 2011, **50**, 5438-5466.

[6] E. Kloser, D. G. Gray, *Langmuir*, 2010, **26,** 13450-13456.

[7] S. Elazzouzi-Hafraoui, J. Putaux, L. Heux, *J. Phys. Chem. B*, 2009, **113**, 11069-11075.

[8] S. Zhang, I. A. Kinloch, A. H. Windle, *Nano Lett*, 2006, **6**, 3.

[9] S.-H. Kim, and D. A. Weitz, *Angew. Chem. Int. Ed.*,, 2011, **50**, 8731 –8734.

[10] S.-H. Kim, J. W. Kim, J.-C. Cho, and D. A. Weitz, *Lab on a Chip*, 2011, **11**, 3162–3166.

[11] A. Abbaspourrad, N. Carroll, S.-H. Kim and D. A. Weitz, *Advanced Materials*, 2013, **135**, 7744−7750.

[12] W. J. Duncanson, A. Abbaspourrad, H. C. Shum, S.-H. Kim, L. Adams and D. A. Weitz, *Langmuir*, 2012**, 27,** 6742-6745.

[13] S.-H. Kim**,** S. Y. Lee, S.-M. Yang and G.-R. Yi., *NPG Asia Materials*, 2011, **3**, 25-33.

[14] G. M. Whitesides, *Nature*, 2006, **442**, 368-373.

[15] A. Utada, L. Chu, A. Fernandez-Nieves, D. Link, C. Holtze, and D.Weitz, *Mrs Bull*, 2007, **32**, 9, 702–708.

[16] H.-L. Liang, E. Enz, G. Scalia and J. Lagerwall, *Mol. Cryst. Liq. Cryst.*, 2011, **549,** 6977.

[17] H.-L. Liang, S. Schymura, P. Rudquist and J. Lagerwall, *Phys. Rev. Lett.*, 2011, **106,** 247801.

[18] H.-L. Liang, R. Zentel, P. Rudquist and J. Lagerwall, *Soft Matter*, 2012, **8**, 5433.

[19] E.-K. Fleischmann, H.-L. Liang, N. Kapernaum, F. Giesselmann, J. Lagerwall and R. Zentel, *Nat. Commun.*, DOI: 10.1038/ncomms2193, 2012.

[20] H.-L.Liang, JH. Noh, R. Zentel, P. Rudquist and J. Lagerwall, *Phil. Trans. R. Soc. A*, 2013, **371,** 20120258.

[21] M. ONeill and S. Kelly, *Adv. Mater.*, 2011, **23**, 566–584.

[22] N. Y. Ha, S. M. Jeong, S. Nishimura and H. Takezoe, *Adv. Mater.*, 2010, **22**, 1617.

[23] N. Ha, Y. Ohtsuka, S. Jeong, S. Nishimura, G. Suzaki, Y. Takanishi, K. Ishikawa and H. Takezoe, *Nat. Mater.*, 2008, **7**, 43–47.

[24] E. Enz, V. La Ferrara and G. Scalia, *ACS Nano*, 2013**, 7**, 6627–6635.

[25] J. D. Davies, Dylan, R. Vaccaro, Antonio, M. Morris, Stephen, N. Herzer, P. H. J. Schenning, Albertus and W. M. Bastiaansen, Cees, *Adv. Funct. Mater.*, 2013, **23**, 2723–2727.

[26] B. E. Sorensen, *Eur J Mineral., 2013***, 25**, *5-10.*

[27] E. Enz, and J. Lagerwall, *J. of Mater. Chem.*, 2010, **20**, 6866-6872.

요 약 (국문 초록)

콜레스테릭(N^*) 액정은 응집 광 물질로 알려져 있으며 독특한 광학적 특성 때문에 광범위한 연구 분야에서 많은 관심을 받고 있다. 자기 조립으로 형성된 주기적인 나선형 구조는 화학 성분이나 온도를 변화시켜 가시광선 스펙트럼 내의 어느 파장의 빛을 반사하게 하도록 그 조절이 가능하다. 특히 콜레스테릭 액정 상에서의 나선형 배열은 나선형과 같은 손잡이의 원 편광된 빛을 반사한다. 여기서 우리는 단분산도의 콜레스테릭 액정 방울과 유리화를 거쳐 얻어진 나노셀룰로오스 필름의 내부적인 콜레스테릭 구조를 통해 두 가지 새로운 콜레스테릭 시스템과 함께 독특한 광학적 특성에 초점을 맞춘다.

동축 미세 유체 시스템을 이용하여 콜레스테릭 혼합물로부터 단분산도의 액정 방울을 생산하였다. 연속상에 분산된 액정 방울은 높은 부피 비율로 모이게 되면 자발적으로 2 차원의 콜로이드 결정 구조로 배열하게 된다. 연속상의 구성성분은 액정 분자의 평면 정렬을 유도하여 나선형 구조의 방사형을 돕는데 이로 인해 전방향의 선택적 반사를 가능하게 하여 특유한 광학적 현상을 일어나게 한다. 우리는 여기서 다채로운 대칭 패턴의 결과로, 액정 방울 사이에서 일어나는 특정한 방식의 광자 간 통신 과정을 설명한다. 근본적인 광학적 관점 외에도 이러한 시스템은 센서 또는 위조방지 태그 등의 응용 분야에 있어 폭넓은 가능성을 지닌다.

나노 셀룰로오스 결정체(CNC)는 현재 상당한 국제적인 관심을 끄는 바이오나노 재료이다. 이는 천연 셀룰로오스 자원에서 추출된 결정화 된

나노 막대 형태이다. 특정 농도에서 CNC 분산액은 콜레스테릭 액정 상을 지니게 되어 결과적으로 나노 막대로 하여금 나선형 구조를 갖게 된다. 우리는 제어된 전단흐름을 이용하여 CNC 분산액을 건조하는 새로운 방법을 개발하여 높은 수준으로 구조적 조절의 얇은 CNC 필름을 제작하였다. 핵심 요소는 용매가 증발하면서 농도가 증가함에 따라 액정 정렬과 맞물려지는 유리화 진행 속도를 낮추는 것이다. 적절한 조건 하에서 건조된 필름은 넓은 범위에서 균일한 무지개 빛깔을 보이고 이는 마이크론 단위 이하의 피치가 균일하게 정렬되었다는 것을 의미한다. 원형 전단흐름을 증가시키면 나선은 풀릴 수 있지만 균일한 복굴절 필름이 생성된다.

.....

주요어: 콜레스테릭 액정, 콜로이드 결정, 자기 조립, 광자 간 통신 (광학적 패턴 형성), 나노 셀룰로오스, 원편광

학 번: 2012-22446